Cement and Concrete Research 40 (2010) 359–369

Contents lists available at ScienceDirect

Cement and Concrete Research

journal homepage: http://ees.elsevier.com/CEMCON/default.asp

Aluminum-rich belite sulfoaluminate cements: Clinkering and early age hydration

M. Carmen Martín-Sedeño [a], Antonio J.M. Cuberos [a], Ángeles G. De la Torre [a], Gema Álvarez-Pinazo [a], Luis M. Ordónez [b], Milen Gateshki [c], Miguel A.G. Aranda [a,*]

[a] Departamento de Química Inorgánica, Cristalografía y Mineralogía, Universidad de Málaga, 29071 Málaga, Spain
[b] Unidad Técnica de Investigación de Materiales, AIDICO, Avda. Benjamín Franklin, 17 Paterna, Valencia, Spain
[c] PANalytical, B.V. P.O. Box 13. 7600 AA Almelo, The Netherlands

ARTICLE INFO

Article history:
Received 9 June 2009
Accepted 13 November 2009

Keywords:
$3CaO \cdot 3Al_2O_3 \cdot CaSO_4$ (D)
Clinkerization (E)
Belite sulfoaluminate cement (D)
Hydration (A)
Quantitative mineralogical phase analysis (B)

ABSTRACT

Belite sulfoaluminate (BSA) cements have been proposed as environmentally friendly building materials, as their production may release up to 35% less CO_2 into the atmosphere when compared to ordinary Portland cements. Here, we discuss the laboratory production of three aluminum-rich BSA clinkers with nominal mineralogical compositions in the range C_2S (50–60%), $C_4A_3\$$ (20–30%), CA (10%) and $C_{12}A_7$ (10%). Using thermogravimetry, differential thermal analysis, high temperature microscopy, and X-ray powder diffraction with Rietveld quantitative phase analysis, we found that burning for 15 min at 1350 ºC was the optimal procedure, in these experimental conditions, for obtaining the highest amount of $C_4A_3\$$, i.e. a value as close as possible to the nominal composition. Under these experimental conditions, three different BSA clinkers, nominally with 20, 30 and 30 wt.% of $C_4A_3\$$, had 19.6, 27.1 and 27.7 wt.%, $C_4A_3\$$ respectively, as determined by Rietveld analysis. We also studied the complex hydration process of BSA cements prepared by mixing BSA clinkers and gypsum. We present a methodology to establish the phase assemblage evolution of BSA cement pastes with time, including amorphous phases and free water. The methodology is based on Rietveld quantitative phase analysis of synchrotron and laboratory X-ray powder diffraction data coupled with chemical constraints. A parallel calorimetric study is also reported. It is shown that the β-C_2S phase is more reactive in aluminum-rich BSA cements than in standard belite cements. On the other hand, $C_4A_3\$$ reacts faster than the belite phases. The gypsum ratio in the cement is also shown to be an important factor in the phase evolution.

1. Introduction

The manufacture of Portland cement produces large amounts of CO_2 due principally to the high calcite ($CaCO_3$) content of the raw mix. Moreover, it needs vast amounts of energy to grind the raw mixtures and the final products. The combined decarbonation, thermal and electrical-power CO_2 emissions may total as much as 0.97 tons of CO_2 per average ton of Portland Cement (OPC) produced. Thus, the cement industry contributes around 6% of all CO_2 anthropogenic emissions [1,2]. Belite-rich cements were proposed as environmentally friendly materials [3,4]. However, the activation of these cements is essential, if they are expected to be used worldwide, due to their slow reaction with water and, consequently, the low mechanical strengths developed at early ages [5]. These disadvantages can be overcome in two complementary ways: i) producing BSA cements, with $C_4A_3\$$ [also named as Klein's salt] [6,7] and ii) stabilizing high temperature belite polymorphs (α-forms) [8–11]. Recently, a class of iron-rich BSA cements has been proposed by Lafarge [12], in which activation is promoted by both strategies already mentioned.[1]

BSA cements can be classified as belite-rich materials, containing more than 50 wt.% of C_2S, while OPC are alite-rich cements with more than 60 wt.% of C_3S [13]. This means that BSA cement production demands less calcium and moreover, part of the calcium carbonate is replaced by calcium sulfate in order to obtain $C_4A_3\$$. BSA cement manufacture in a modern cement plant can give CO_2 emission reductions of up to ~35% per mass of cement produced, relative to OPC, as a result of i) less limestone in the raw feed; ii) a lower burning-zone temperature, (~1250 °C, as opposed to ~1450 °C for OPC and iii) ease of cement grinding due to higher clinker porosity [14,15].

The most common formulation of BSA cements is C_2S, $C_4A_3\$$ and C_4AF [6,12,14,16,17]. These are iron-rich BSA cements produced at ~1250 °C and they are characterized by rapid hardening, excellent durability, self-stressing and volume stability, depending on the amount of gypsum added [18]. Alternatively, in order to further enhance mechanical strengths at very early ages, i.e. <1 day, C_4AF phase may be substituted by $C_{12}A_7$, although an increase of ~100 °C in the maximum

* Corresponding author. Tel.: +34 952131874; fax: +34 952132000.
E-mail address: g_aranda@uma.es (M.A.G. Aranda).

[1] Cement nomenclature is used: C = CaO, S = SiO_2, A = Al_2O_3, F = Fe_2O_3, $\$ = SO_3 and H = H_2O.

0008-8846/$ – see front matter © 2009 Elsevier Ltd. All rights reserved.
doi:10.1016/j.cemconres.2009.11.003

burning temperature is needed and the durability with respect to sulfate attack is limited [19,20]. This formulation relies on the equilibrium system C_2S–C_4A_3–$C_{12}A_7$–CA [21] where aluminate phases and C_4A_3\$ are responsible for the early strength development, while the C_2S provides good secondary hardening. Cements from this chemical system would combine calcium aluminate cement and sulfoaluminate cement performances. Whatever the formulation proposed, some questions about the clinker formation process remain open. For instance, the avoidance of the formation of some non-hydraulic phases, such as C_2AS or C_5S_2\$ [22,23] at the expense of C_4A_3\$.

BSA cement hydration is a complex process, but there is already a significant amount of literature on the subject [24,25]. Therefore, advanced techniques and chemical tools must be developed in order to better understand BSA cements hydration. X-ray powder diffraction (XRPD) is an appropriate technique to identify, quantify and characterize the crystalline phase(s) involved in the hydration reactions. The application of Rietveld methodology [26] to XRPD data in order to obtain quantitative phase analyses (QPA) has been demonstrated for anhydrous cement materials [27–31], including the quantification of the amorphous fraction by adding a suitable standard [32]. Attempts to quantify the hydration processes of cements using XRPD and the Rietveld method have also been published in the last few years [33,34]. The results obtained have shown the complexity of the hydration reactions mechanism even for pure synthetic clinker phases [35]. This complexity does not derive solely from the great variety of hydrated compounds, amorphous and crystalline, but also because certain phases (AFm phases) are difficult to quantify (and even to identify) due to their low crystallinity and sometimes polytypism. Furthermore, variations in composition (e.g. hydration degree) with the corresponding changes in their powder patterns (both in the position and intensity of the peaks) may take place during the hydration of the cements, mainly for aluminate hydrates [36].

In spite of the complexity of the hydration reactions, some details about the hydration mechanisms in the system C_4A_3\$–C\$$H_2$–$H_2O$ are well-established [37]. Furthermore, the hydration reactions of BSA cement pastes at early stages, 24 h, have already been studied at different temperatures (25, 55, 85 °C) by calorimetry and XRPD [25]. However, QPA of the hydrated compounds were not performed. Despite the abundant literature on cement hydration, not all details of the hydration process have been clarified yet, in particular, the structural and chemical features of the first hydrous phases including a detailed study of the different chemical reactions.

Here, we present a study of the clinker formation processes for aluminum-rich BSA clinkers containing C_2S, C_4A_3\$, $C_{12}A_7$ and CA as the main phases. We have determined the temperature and time of residence in the kilns to obtain an appropriate phase assemblage by X-ray diffraction jointly with the Rietveld method [26], among other techniques. Moreover, this work reports the results of hydration of aluminum-rich BSA cements. The hydration process of these BSA cements has been followed by *in-situ* synchrotron and laboratory X-ray powder diffraction [SXRPD, LXRPD], Rietveld methodology and chemical constraints. This last study is carried out in order to determine the hydration behavior in general and the role of gypsum, in particular. A calorimetric study is also presented.

2. Experimental section

2.1. Material preparations

2.1.1. Synthesis of BSA clinkers

Table 1 gives the nominal dosages, expressed as oxide, of the raw mixtures used to prepare the BSA clinkers. To fabricate those raw mixtures, 25–30 wt.% of Kaolin (Aldrich), 3–9 wt.% of γ-Al_2O_3 (99.997% AlfaAesar), 60–64 wt.% of calcium carbonate (99.95–100.05% AlfaAesar) and 4–6 wt.% of pure gypsum were mixed. Theoretical mineralogical composition and nomenclature of BSA clinkers are also given in Table 1, where the numbers stand for the theoretical amounts of β-C_2S and C_4A_3\$, for instance, BSA_60:20, means a clinker with 60 wt.% of β-C_2S and 20 wt.% of C_4A_3\$, theoretical compositions. Raw materials were mixed by hand in an agate mortar with the aid of absolute ethanol and dried in an oven at 60 °C. This treatment was performed by triplicate. Various raw materials mixtures were pressed into pellets ~20 mm in diameter weighing ~3 g. The pellets were placed into Pt/Rh crucibles and calcined at 900 °C for 30 min after ramping up at a heating rate of 5 °C/min. Then, the temperature was raised at the same rate to the final temperature (1250 °C, 1300 °C or 1350 °C) and held for 15 or 30 min at the given temperature. Finally, the clinkers were quenched from this temperature by opening the furnace and taking the crucibles out and simultaneously applying air flow using a dryer. We obtained ~15 g of each clinker which were finely ground by hand with a tungsten carbide mortar and pestle to pass through a 100 μm sieve prior to powder diffraction measurements.

Table 1
Nominal elemental composition of raw mixtures (expressed as oxides, wt.%) and theoretical mineralogical composition (wt.%) of BSA clinkers.

	CaO	SiO_2	Al_2O_3	SO_3	C_2S	C_4A_3\$	$C_{12}A_7$	CA
BSA_60:20	54.82	20.93	21.62	2.62	60	20	10	10
BSA_60:30	54.30	20.93	20.84	3.94	60	30	5	5
BSA_50:30	51.99	17.44	26.64	3.94	50	30	10	10

2.1.2. Preparation of BSA cements

BSA cements were prepared by mixing selected BSA clinkers (prepared as in section 2.1.1.) with different dosages of gypsum. The added amounts of gypsum were: 5, 10 and 15 wt.% to BSA_60:20 and BSA_50:30. The cements are hereafter labeled as C*x*BSA_60:20 or C*x*BSA_50:30 where $x = 5$, 10 or 15 stands for the percentage of gypsum added to the clinkers. The Blaine parameters obtained for all cements were: C5BSA_60: 20485 m^2/kg, C10BSA_60: 20551 m^2/kg, C15BSA_60: 20471 m^2/kg, C5BSA_50:30423 m^2/kg, C10BSA_50: 30502 m^2/kg and C15BSA_50: 30470 m^2/kg.

2.2. Analytical techniques

2.2.1. Laboratory X-ray powder diffraction (LXRPD)

2.2.1.1. LXRPD for BSA clinkers. LXRPD data were recorded on an X'Pert MPD PRO diffractometer (PANalytical) using strictly monochromatic CuKα_1 radiation ($\lambda = 1.54059$ Å) [Ge (111) primary monochromator] and working in reflection geometry ($\theta/2\theta$). The optics configuration was a fixed divergence slit (1/2°), a fixed incident antiscatter slit (1°), a fixed diffracted anti-scatter slit (1/2°) and X'Celerator RTMS (Real Time Multiple Strip) detector, working in scanning mode with maximum active length. Data for each sample were collected from 10° to 70° (2θ) during ~2 h. The samples were rotated during data collection at 16 rpm in order to enhance particle statistics. The X-ray tube worked at 45 kV and 35 mA.

2.2.1.2. LXRPD for BSA cement pastes. LXRPD *in-situ* hydration study for the C*x*BSA_60:20 ($x = 5$, 10 and 15) and C5BSA_50:30 cements were performed at the application laboratory of PANalytical in Almelo (The Netherlands) with an X'Pert PRO MPD diffractometer in transmission geometry with θ/θ goniometer, using CuK$\alpha_{1,2}$ radiation ($\lambda = 1.5418$ Å) and using a focusing X-ray mirror. This optical component is able to transform the divergent X-ray beam from a tube in line focus position to an intense beam that focuses onto the goniometer circle. The optics configuration was a fixed divergence slit (1/2°), a fixed incident antiscatter slit (1/2°), a Nickel filter of 0.020 mm in the diffracted beam path and a PIXcel RTMS (Real Time Multiple Strip) detector, working in scanning mode with full active length. Each pattern was collected from 5º to 55° (2θ) in repetition mode (three times) with total duration of ~0.4 h at selected times of hydration. The samples were

rotated during data collection at 16 rpm in order to enhance particle statistics. The X-ray tube worked at 45 kV and 40 mA. Small batches of cement pastes were prepared by hand-mixing 0.10 g of cement with 0.05 g of water, and immediately spread between two Kapton foils in the sample holder. The actual size of the paste samples was ~10.0 mm diameter × ~0.3 mm thickness.

2.2.2. Synchrotron X-ray powder diffraction

SXRPD *in-situ* hydration studies were performed on the BM08 [Italian CRG "GILDA"] beamline of the European Synchrotron Radiation Facility, ESRF (Grenoble, France) in Debye–Scherrer (transmission) configuration for C10BSA_50:30. An image plate (IP) detector [38] was used working in two configurations: i) Translating mode (for the first 4 h of hydration): the IP moves behind two slits with a constant speed and the diffraction pattern is recorded as a function of time. The slits select a vertical slice of the diffraction rings. The translation speed and the slit size can be chosen to fit the experimental requirements. The distance from IP to the sample was 217.0 mm. ii) 2D pattern (for later ages, i.e. >4 h): the slits are removed and the whole diffraction rings are collected during 5 min. The images recorded (in both configurations) in the IP detector were recovered using a Fuji BAS2500 laser scanner (16 bit/pixel with a minimum pixel size of 50 × 50 μm). The SXRPD patterns obtained in translating mode were extracted in 5 min slices using original software available at BM08. Powder patterns from 2D images were obtained by integration of the rings using FIT2D software [39]. The wavelength used was λ = 0.6888 Å (18.00 keV) and calibrated with Si NIST (a = 5.431195 Å). C10BSA_50:30 paste was prepared *ex-situ* by mixing cement with water at w/c = 0.5 and was immediately loaded in a cylindrical polycarbonate sample holder (15.0 mm diameter × 1.2 mm height) covered over both sides with Kapton slices. The sample holder was spun during data collection to improve the particle statistics and hence to obtain good QPA. The temperature within the experimental hutch was 20 ± 2 °C.

2.2.3. XRPD data analysis

LXRPD patterns of clinkers were analyzed by the Rietveld method with GSAS software package [40] by using a *pseudo*-Voigt peak shape function [41] with the asymmetry correction included [42]. The refined overall parameters were: background coefficients, cell parameters, zero-shift error, peak shape parameters and phase fractions. The structural descriptions used for fitting the anhydrous crystalline phases within the clinkers are given in Table 2 (including the Inorganic Crystal Structure Database, ICSD, collection codes).

SXRPD and LXRPD patterns of cement pastes were analyzed by the Rietveld method with X'Pert Highscore Plus software from PANalytical B.V., version 2.2d. The refined overall parameters were: cell parameters, zero-shift error, W (Gaussian contribution) peak shape parameter and phase fractions. Background function was manually established using the base point tool of the software. Peak shapes were fitted by using the *pseudo*-Voigt function [42]. Table 3 gives the bibliographic references and ICSD collection codes for the structural descriptions of all hydrated crystalline phases.

Table 2
Bibliographic information and ICSD collection codes for all anhydrous crystalline phases.

	Reference	ICSD code
β-C_2S	[43]	81096
γ-C_2S	[44]	200707
$C_4A_3\$$ (ort)	[45]	80361
$C_4A_3\$$ (cub)	[46]	9560
CA	[47]	260
$C_{12}A_7$	[48]	241243
CA_2	[49]	16191
C_3A	[50]	1841
C_2AS	[51]	31235
C	[52]	61550
C$	[53]	16382

Table 3
Bibliographic information and ICSD collection codes for all hydrated crystalline phases.

	Reference	ICSD code
$C\$H_2$	[54]	151692
AFt	[55]	155395
AFm-12 [$C_4A\$H_{12}$]	[56]	100138
CAH_{10}	[57]	407150
C_2AH_8	See text	–
AH_3	[58]	6162
C_2ASH_8	[59]	69413

2.2.4. High temperature microscopy (HTM)

The thermal behavior of BSA raw materials was analyzed by high temperature microscopy (HTM). The BSA_60:20 raw mix was selected to perform this study on a Leica (Wetzlar, Germany) system with automatic image analysis (EMI-version 1.5). The temperature was varied from RT up to 1525 °C at a heating rate of 5 °C/min.

2.2.5. Thermal analysis

Thermogravimetric and differential thermal analyses (TG-DTA) were performed on raw mixtures using a Netzsch STA 409 equipped with TASC 414/2 controller. The temperature was varied from RT up to 1450 °C at a heating/cooling rate of 5 °C/min with a flux of air.

2.2.6. Scanning electron microscopy (SEM)

Pieces of clinker pellets were examined using a JEOL SM 840 scanning electron microscope. The samples were metalized by gold sputtering for better image definition.

2.2.7. Isothermal calorimetric study

The isothermal calorimetric study was performed for C5BSA_60:20, C10BSA_60:20, C5BSA_50:30 and C10BSA_50:30 in an eight channel Thermal Activity Monitor (TAM) instrument using glass ampoules. Pastes were prepared by mixing ~6 g of cement with water at a w/c ratio of 0.5, and the heat flow was collected up to 110 h at 20 °C.

3. Results and discussion

3.1. Determination of temperature and time for clinkering

Fig. 1a and b shows, respectively, the TG and DTA curves for the BSA_60:20 raw mix, (selected as an example). Fig. 1a shows

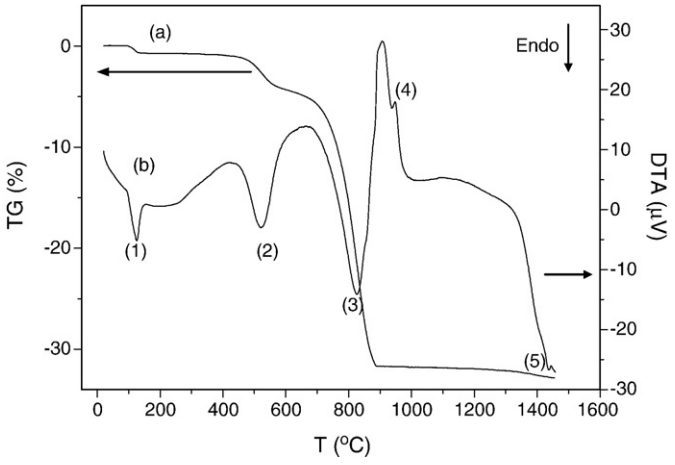

Fig. 1. Thermogravimetric (a, left) and differential thermal analysis (b, right) curves for BSA_60:20 raw mixture. Main effects are highlighted and discussed in the text.

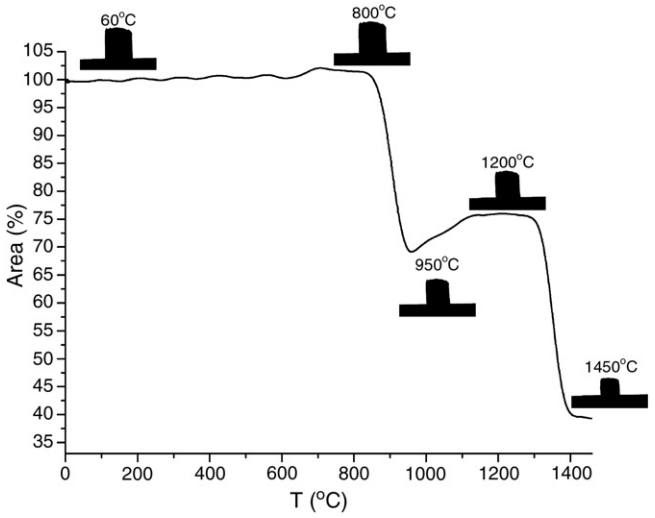

Fig. 2. High-temperature microscopy plot showing area changes of the projected cylinder image of BSA_60:20 raw mixture as a function of temperature.

decarbonation as the main weight loss, as expected Fig. 1b displays a number of thermal effects. Two small endothermic peaks, corresponding to a weight loss resulting from the dehydration of gypsum and dehydroxylation of kaolin, are observed at ~100 °C and ~500 °C, respectively (points 1 and 2). The theoretical weight losses due to gypsum and kaolin are 0.8 and 3.9 wt.%, respectively, while the experimental values were 0.7 and 3.8 wt.%. The strong endotherm at ~800 °C (point 3), with an associated weight loss of 27.2 wt.%, is due to the decomposition of $CaCO_3$, (the theoretical value was 27.7 wt.%). The sharp exothermic peak at ~940 °C (point 4) corresponds to the coordination change of aluminum in meta-kaolin (amorphous) during its transformation into a spinel-like transient phase prior to the formation of mullite [60,61]. Finally, the curve includes another small endothermic peak at ~1440 °C (point 5). This last effect corresponds to the $\alpha'_H \rightarrow \alpha$ belite transformation upon heating [62]. This peak is within a large downward trend likely due to partial melting of the aluminate phases and also to $C_4A_3\$$ partial decomposition.

Fig. 2 shows one of the results obtained in the HTM study. The graph represents area changes of the projected cylinder image as a function of temperature for BSA_60:20 raw mixture. We observed a contraction of the sample between 850 and 950 °C due to the decomposition of $CaCO_3$ and the formation of the corresponding oxide. Between 950 and 1150 °C a significant expansion took place, presumably due to the occurrence of expansive chemical reactions likely related to the formation of calcium aluminates [4]. Between 1150 and 1300 °C, the area stays relatively constant. Finally, a sharp decrease of the projected area is observed above ~1300 °C due to sintering processes and possibly to the undesirable formation of a significant amount of liquid phase.

3.2. Rietveld quantitative phase analysis (RQPA) of BSA clinkers

BSA clinkers are complex materials due to the presence of many crystalline phases and, moreover, some of these components display polymorphism. Table 4 shows RQPA for BSA_60:20 clinker at different temperatures and times of residence at that temperature, as well as the Rietveld agreement factor for the refinements. Rietveld results are normalized to 100% of crystalline phases (*i.e.* the presence of an amorphous/non-diffracting fraction is not taken into account). Inspecting the data in Table 4, it has to be highlighted that the percentage of free lime is lower than 2 wt.% for all tests. This fact indicates that the main clinker formation processes are finished at ~1250 °C. However, at this temperature (1250 °C) the amount of $C_4A_3\$$ is lower than that obtained at 1350 °C, so the production of these BSA clinkers should be between

Table 4
Rietveld quantitative phase analysis results of BSA_60:20 clinker, at different temperatures and times of clinkering, in wt.% obtained from LXRPD data. Agreement factors (R_{WP}) for the final refinements are also given.

	1250 °C		1300 °C		1350 °C	
	15 min	30 min	15 min	30 min	15 min	30 min
β-C_2S	57.0(1)	53.8(1)	54.8(1)	54.8(1)	55.8(1)	57.3(1)
$C_4A_3\$$	17.0(1)	16.8(1)	18.3(1)	18.5(1)	19.6(1)	19.0(1)
$C_{12}A_7$	13.2(1)	14.6(1)	15.2(1)	14.7(1)	13.5(1)	14.7(1)
CA	4.2(2)	1.9(1)	2.0(1)	1.9(1)	4.4(2)	5.4(1)
C_2AS	5.2(1)	9.8(1)	7.8(1)	7.5(1)	4.3(1)	1.5(1)
CA_2	1.6(1)	0.4(1)	–	–	–	–
CaO	0.8(1)	1.4(1)	0.7(1)	0.7(1)	–	–
γ-C_2S	–	–	–	0.6(1)	1.9(1)	2.1(1)
C_3A	1.1(1)	1.3(1)	1.2(1)	1.3(1)	0.5(1)	–
R_{WP}/%	7.3	6.7	6.5	6.9	6.2	6.2

1300 and 1350 °C. On the other hand, all the tested procedures yielded clinkers with non-negligible percentages of gehlenite (C_2AS). C_2AS is described as intermediate phase in the mechanism of formation of these clinkers [63,64]. In reference [65], a factor *P*, (= A/$), was defined, and it was stated that clinkers with $P = 3.82$ or lower at 1300 ºC do not contain C_2AS but those with *P* over 3.82 may have some. Furthermore, gehlenite can remain above 1200 °C [66] in calcium aluminate cements (CACs). The *P* values for clinkers BSA_60:20, BSA_60:30 and BSA_50:30 are 8.3, 5.3 and 6.8, respectively. Consistent with the above references, C_2AS was observed in all of these clinkers.

Small amounts of the low-temperature polymorph of dicalcium silicate, γ-C_2S, were also found. This phase is formed on cooling by the polymorphic transformation, β-$C_2S \rightarrow$ γ-C_2S, but it is hydraulically inactive and therefore its presence is undesirable in clinkers. The formation of γ-C_2S is enhanced by i) prolonged holding times at high temperatures, ii) low cooling rates and iii) the absence of foreign ions such as sodium or potassium [13] which could stabilize the β-form. The presence of γ-C_2S phase in these laboratory BSA clinkers is associated mainly with iii). Final clinker mineralogical compositions were almost the same for the two high temperature holding times tested, so the shorter time would be the best option in practice for obvious environmental and economic reasons. Fig. 3 shows the Rietveld plot for BSA_60:20 prepared at 1350 °C for 15 min as an example, with the major peaks for each phase

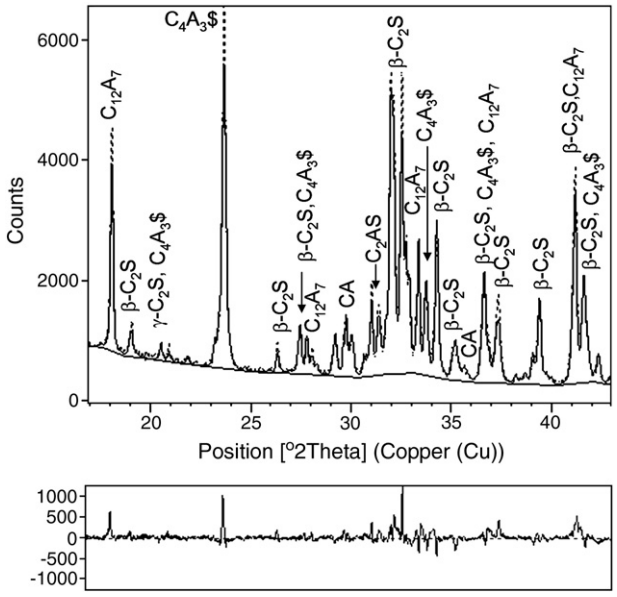

Fig. 3. Selected range of the Rietveld plot for BSA_60:20 clinker. Dots are the experimental scan, solid line is the calculated pattern and the bottom line is the difference curve. The major peaks for each phase are labeled.

Table 5
Quantitative phase analysis results (wt.%) for the clinkers obtained at the final conditions (1350 ºC for 15 min) determined from the Rietveld study. Nominal (expected) compositions are given in italics for comparison. Agreement factors (R_{WP}) for the final refinements are also given.

Phases	BSA_60:20		BSA_60:30		BSA_50:30	
β-C_2S	55.8(1)	60	59.5(1)	60	52.1(1)	50
$C_4A_3$$	19.6(1)	20	27.7(1)	30	27.1(1)	30
$C_{12}A_7$	13.5(1)	10	8.1(1)	5	3.0(1)	10
CA	4.4(2)	10	1.6(1)	5	5.2(1)	10
C_2AS	4.3(1)	–	0.5(1)	–	1.8(1)	–
CA_2	–	–	0.7(1)	–	2.8(2)	–
C_3A	0.5(1)	–	1.1(1)	–	8.0(1)	–
γ-C_2S	1.9(1)	–	0.9(1)	–	–	–
R_{WP}/%	6.2		6.2		7.4	

labeled. RQPA, HTM and TG-DTA results show that 15 min at 1350 °C is an appropriate burning condition for making these aluminum-rich BSA clinkers. To avoid the decomposition of Klein's phase, the clinkering temperature should not be higher than 1350 °C [67].

Two other BSA clinkers, BSA_60:30 and BSA_50:30, were prepared following the procedure determined above: 15 min at 1350 °C. The elemental and theoretical mineralogical compositions are given in Table 1. RQPA were performed for these two clinkers in order to follow the clinker formation process — see Table 5. The percentages of main phases (C_2S and $C_4A_3$$) were quite close to the expected values, although some minor mineralogical components were also observed in all of these clinkers.

The main objective of this study is to obtain "environmentally–friendly" clinkers. The methodology proposed here to manufacture these aluminum-rich BSA clinkers reduces CO_2 emissions from the reduction of calcite in the raw feed. For the production of a ton of an ordinary Portland clinker with 60 wt.% of C_3S, 20 wt.% of C_2S, 12 wt.% of C_4AF and 8 wt.% of C_3A, 1.2 tons of calcite are used releasing 0.53 tons of CO_2 into atmosphere. The production of the BSA clinkers proposed in this study, i.e. BSA_60:20, BSA_60:30, BSA_50:30, needs 0.95, 0.92 and 0.88 tons, respectively, of calcite. The reductions of CO_2 arising from the decarbonation of calcite, compared to that of OPC, are 20.8, 24.5 and 26.4 wt.%, respectively. These numbers arise only from the reduction of the amount of calcite used in the process, but in parallel, there are similar reductions in the amount of fuel required for this highly endothermic reaction. Furthermore, the reduction of 100 °C in the clinkering temperature will permit a small reduction of CO_2 coming from fuel as a result of reduced kiln shell heat losses. Another aspect to be borne in mind is the milling processes of clinker. It is known that belite-rich clinkers without $C_4A_3$$ are more difficult to mill than ordinary Portland clinkers [2]. However clinkers with Klein's salt are often more porous, due to the negligible/small amount of liquid phase formed in the burning process, and easier to grind [68,69]. We have performed a SEM study of pieces of clinker pellets (without milling) in order to examine the texture of the clinkers. Fig. 4 shows the SEM photographs of (a) a belite-rich clinker [10] and (b) BSA_50:30, prepared under the conditions detailed in this work. From these images, it is clear than BSA clinkers are more porous than belite-rich clinkers, which should favor their grindability, as already reported [68,69].

3.3. Rietveld quantitative phase analysis (RQPA) of cement pastes

All hydrated cements were measured continuously during the first hours of hydration. After that time, isolated patterns were collected to study later ages. Fig. 5 shows, as an example, the time-resolved LXRPD patterns for C5BSA_60:20 paste during the first 8 h [20 patterns collected each 24 min (8 min/pattern × 3 repetitions)]. In these first hours of hydration, some changes in the phase assemblage were observed. For instance, the diminution of Klein's salt and the appearance of ettringite can be observed, and their diffraction peaks are labeled with a plus symbol and an asterisk, respectively. Initially

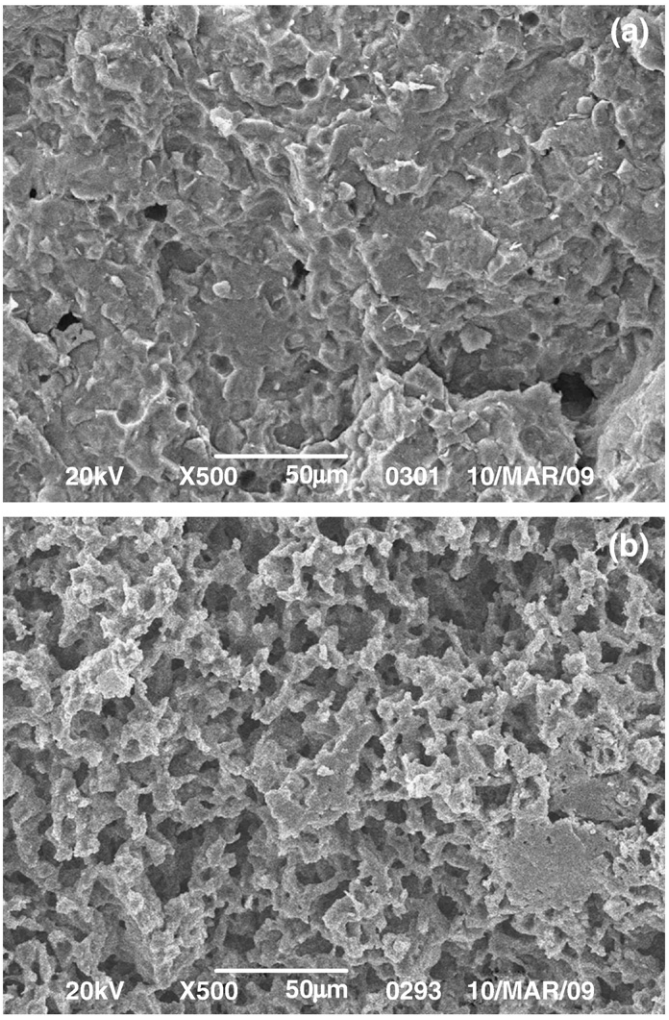

Fig. 4. SEM photographs for (a) belite-rich clinker and (b) BSA_50:30 clinker.

C_2AH_8 was also formed, but at later ages it starts to react and finally disappears. This evolution with time is highlighted by a dashed line in Fig. 5. All the patterns were analyzed in order to identify the mineralogical phases that were appearing, and RQPA was performed for selected times of hydration. Tables 6–9 give the direct Rietveld results for all the cement pastes studied. In these tables, initial anhydrous phase assemblages are included, (t_0). All the cements contain $C_{12}A_7$ which reacts very quickly, as expected. On the other hand, $C_4A_3$$ and CA hydration kinetics are relatively slow. C_2AS does not react with water at room temperature, and β-C_2S phase is hydraulically inactive at early ages. As a consequence, their percentages should be invariable. RQPA percentages for β-C_2S and C_2AS appear to increase with time, (Tables 6–9). However, it should be noted that RQPA results are normalized to 100 wt.% of crystalline phases.

Three main points characterize the hydration process: i) disappearance of crystalline anhydrous phases; ii) appearance of both amorphous and crystalline hydrate phases; and iii) diminution of free water. Since RQPA results are normalized to 100 wt.% of crystalline phases, the percentages of slowly-hydrating anhydrous phases such as β-C_2S, appear to increase during hydration due to the overall decrease of crystalline phases within the probed volume. Hence, in order to fully extract all the information about the hydration of cement pastes, the direct RQPA results need to be normalized to include the amorphous phases and free water. The methodology used here is based on the assumption that one crystalline phase remains unreacted from one powder pattern to the next. At early ages β-C_2S is assumed not to react, so

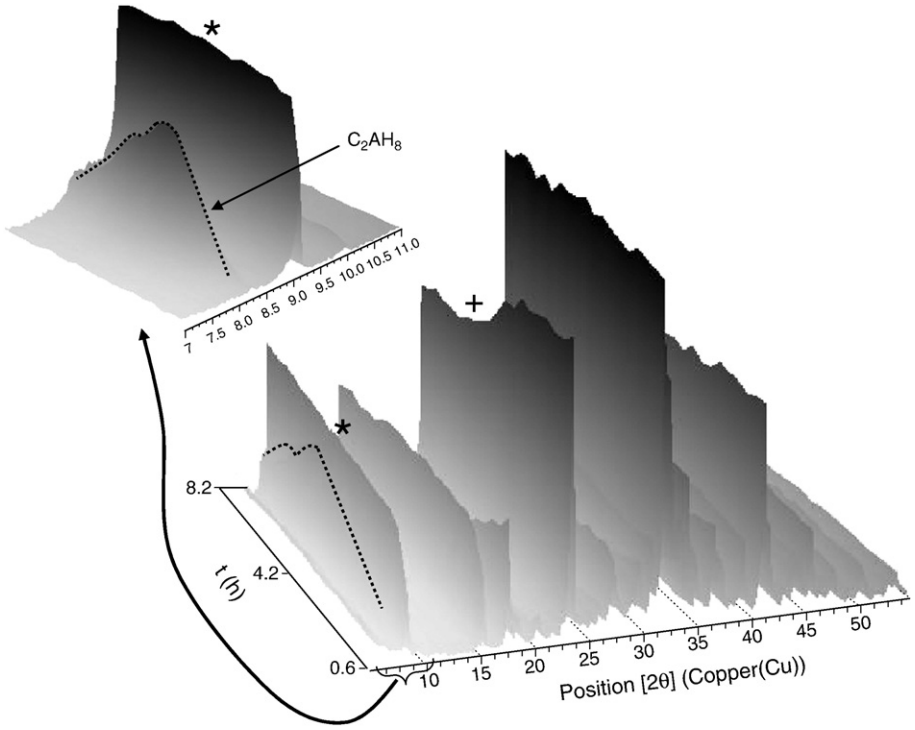

Fig. 5. Time-resolved LXRPD raw data for C5BSA_60:20 cement hydration during the first hours. The inset shows an enlarged selected region (7–11°/2θ) for the same composition. Ettringite and Klein's salt main diffraction peaks are labeled with an asterisk and plus symbol, respectively. C_2AH_8 evolution with time is highlighted by a dashed line.

Table 6
Direct RQPA results for the hydration of C5BSA_60:20 paste from LXRPD data.

	t_0	$t_{0.6}$	$t_{2.2}$	$t_{4.2}$	$t_{6.2}$	$t_{8.2}$
	0.0 h	0.6 h	2.2 h	4.2 h	6.2 h	8.2 h
β-C_2S	55.1(1)	53.8(3)	54.4(3)	57.0(4)	59.3(4)	60.5(4)
$C_4A_3\$$	18.6(1)	18.7(2)	18.3(2)	16.8(2)	14.7(2)	14.9(2)
$C_{12}A_7$	16.3(1)	13.1(2)	7.9(2)	1.3(2)	1.4(1)	1.4(2)
CA	3.4(1)	3.2(2)	2.4(1)	1.5(1)	1.1(1)	1.2(1)
C_2AS	1.6(1)	1.0(1)	1.4(1)	2.7(1)	3.0(2)	3.2(2)
$C\$H_2$	5.0(−)	1.6(1)	–	–	–	–
AFt	–	8.6(2)	14.1(3)	14.9(2)	16.2(3)	16.2(3)
AFm-16	–	–	0.4(1)	1.7(2)	1.2(2)	0.3(1)
C_2AH_8	–	–	1.2(2)	4.0(2)	3.0(2)	2.3(3)

β-C_2S percentage and Rietveld results are used to infer the amounts of the other phases that are reacting. However, this assumption is not true at later ages, e.g. later than ~30 h for C10BSA_50:30 paste. Therefore, we have adopted an alternative methodology to carry out the normalization of the RQPA for C10BSA_50:30. After inspecting direct RQPA for this paste, Table 9, C_2AS phase, which is hydraulic inactive, has been assumed to be constant to normalize data after 33.8 h. Once the percentage of a reacting phase is obtained, the stoichiometric reactions are considered.

3.4. Normalization of RQPA results

The normalization procedure given just below was performed on four cement pastes, one measured with SXRPD and three with LXRPD. As this is a new methodology, it is advisable to start using a technique with lowest associated errors, i.e. high resolution penetrating synchrotron X-ray powder diffraction, which overcomes most of the drawbacks of LXRPD [27]. However, once the methodology is established it can be extended to laboratory X-ray powder diffraction, a much more accessible technique.

The initial ($t = 0.0$ h) phase assemblage of each cement paste is 66.7 wt.% of anhydrous cement and 33.3 wt.% of free water ($w/c = 0.5$). Figs. 6–9 show the normalized Rietveld results for all the cements studied. The normalization was performed step by step from a certain hydration time to the following one. To do so, two sets of data are considered in each step: normalized phase assemblage at t_x (including free water and amorphous phases) and direct Rietveld phase assemblage at t_y, were x

Table 7
Direct RQPA results for the hydration of C10BSA_60:20 paste from LXRPD data.

	t_0	$t_{0.7}$	$t_{1.7}$	$t_{2.7}$	$t_{3.2}$	$t_{5.2}$	$t_{8.7}$	$t_{14.2}$	$t_{15.2}$
	0.0 h	0.7 h	1.7 h	2.7 h	3.2 h	5.2 h	8.7 h	14.2 h	15.2 h
β-C_2S	52.1(1)	50.4(4)	49.5(4)	49.5(4)	50.0(4)	51.6(4)	51.5(4)	51.4(4)	51.9(4)
$C_4A_3\$$	17.6(1)	17.5(3)	14.8(2)	12.5(1)	11.9(2)	12.0(2)	12.2(2)	12.0(2)	12.1(2)
$C_{12}A_7$	15.5(1)	12.4(2)	3.4(2)	2.2(2)	1.8(2)	1.7(1)	1.9(2)	2.0(2)	2.0(2)
CA	3.2(1)	2.6(2)	2.1(2)	1.6(2)	1.7(2)	1.3(1)	1.8(2)	2.2(2)	2.1(2)
C_2AS	1.5(1)	0.9(1)	1.7(2)	2.4(2)	2.5(2)	1.9(1)	1.9(1)	2.2(1)	1.9(1)
$C\$H_2$	10.0(−)	5.9(2)	1.4(1)	1.2(1)	1.4(1)	1.6(1)	1.5(1)	1.7(1)	1.8(1)
AFt	–	10.3(2)	25.2(3)	27.8(3)	28.0(3)	28.9(3)	29.0(3)	28.4(3)	28.1(3)
AFm-16	–	–	0.7(2)	1.1(4)	0.9(3)	0.5(1)	–	–	–
C_2AH_8	–	–	1.3(1)	1.8(3)	1.9(3)	0.5(2)	0.2(1)	0.2(1)	0.2(1)

Table 8
Direct RQPA results for the hydration of C5BSA_50:30 paste from LXRPD data.

	t_0	$t_{0.5}$	$t_{1.3}$	$t_{2.1}$	$t_{2.9}$	$t_{4.1}$	$t_{15.3}$	$t_{16.9}$
	0.0 h	0.5 h	1.3 h	2.1 h	2.9 h	4.1 h	15.3 h	16.9 h
β-C_2S	50.0(1)	44.8(3)	45.5(3)	46.3(3)	45.2(3)	46.5(3)	53.7(4)	53.6(3)
C_4A_3\$	25.4(1)	25.8(3)	25.5(3)	25.7(3)	26.6(3)	26.4(3)	20.2(3)	20.5(3)
$C_{12}A_7$	9.0(1)	5.8(2)	4.2(2)	2.9(2)	1.9(2)	0.8(1)	0.5(1)	0.4(1)
CA	4.1(1)	4.6(2)	4.0(2)	4.1(2)	3.9(2)	3.0(2)	1.4(1)	1.5(1)
C_3A	2.3(1)	1.6(2)	2.1(2)	2.1(1)	1.8(1)	1.6(1)	1.1(1)	1.0(1)
C_2AS	2.7(1)	2.1(1)	2.4(2)	2.7(2)	2.6(2)	2.7(2)	3.6(2)	3.7(1)
CA_2	1.6(1)	1.1(2)	1.1(2)	1.0(2)	1.0(2)	1.1(2)	0.7(2)	1.0(2)
C\$$H_2$	5.0(–)	0.6(1)	0.3(1)	–	–	–	–	–
AFt	–	13.7(4)	14.4(4)	14.0(3)	15.1(4)	15.4(4)	16.6(4)	16.1(4)
AFm-16	–	–	0.3(1)	0.3(1)	0.6(1)	0.6(1)	0.5(1)	0.3(1)
C_2AH_8	–	–	0.3(1)	0.8(1)	1.3(1)	1.9(1)	0.6(2)	0.8(2)
CAH_{10}	–	–	–	–	–	–	1.3(1)	1.2(1)

Table 9
Direct RQPA results for the hydration of C10BSA_50:30 paste from SXRPD data.

	t_0	$t_{0.9}$	$t_{3.8}$	$t_{7.8}$	$t_{8.5}$	$t_{33.8}$	$t_{57.6}$
	0.0 h	0.9 h	3.8 h	7.8 h	8.5 h	33.8 h	57.6 h
β-C_2S	47.3(1)	46.1(4)	44.9(3)	45.5(3)	46.7(3)	43.4(4)	44.0(3)
C_4A_3\$	24.0(1)	22.9(3)	21.1(2)	20.7(2)	3.4(2)	2.8(2)	3.0(2)
$C_{12}A_7$	8.6(1)	4.4(1)	1.7(1)	0.8(1)	–	–	–
CA	3.9(1)	4.0(2)	3.8(2)	2.6(2)	0.8(1)	0.4(2)	0.3(2)
C_3A	2.2(1)	0.4(1)	0.4(1)	0.4(1)	–	–	–
C_2AS	2.5(1)	2.3(1)	1.9(2)	2.1(1)	3.3(2)	3.3(2)	3.2(2)
CA_2	1.5(1)	1.3(3)	1.6(2)	1.3(2)	1.2(3)	–	–
C\$$H_2$	10.0(–)	2.5(1)	0.8(1)	0.7(1)	–	–	–
AFt	–	16.0(3)	23.8(3)	24.8(3)	32.1(4)	32.6(4)	32.8(4)
AFm-16	–	–	–	–	3.3(1)	1.1(2)	–
AFm-12	–	–	–	–	1.2(1)	1.5(2)	1.5(2)
AFm-14	–	–	–	–	3.9(2)	3.9(2)	4.0(2)
C_2AH_8	–	–	–	1.2(1)	1.8(1)	0.3(1)	–
AH_3	–	–	–	–	2.2(1)	1.9(1)	1.7(1)
C_2ASH_8 C\$$H_2$	–	–	–	–	–	8.7(2)	9.5(2)

and y stands for hours of hydration and always $x<y$. For example, to obtain normalized RQPA at $t_{0.6}$ for C5BSA_60:20, normalized RQPA at t_0 (the previous time) is used. Thus, normalized phase assemblage at t_0 is: 36.7 wt.% of β-C_2S, 12.4 wt.% of C_4A_3\$, 10.9 wt.% of $C_{12}A_7$, 2.3 wt.% of CA, 1.1 wt.% of C_2AS, 3.3 wt.% of gypsum and 33.3 wt.% of free water. On the other hand, $t_{0.6}$ direct Rietveld results are given in Table 6. During the first hour ettringite (AFt) is the only crystalline hydrate observed to form, presumably according to the following reactions:

$$C_{12}A_7 + 12C\$H_2 + 113H \rightarrow 4C_6A\$_3H_{32} + 3AH_3 \quad (1)$$

$$3CA + 3C\$H_2 + 32H \rightarrow 4C_6A\$_3H_{32} + 2AH_3 \quad (2)$$

$$C_4A_3\$ + 2C\$H_2 + 34H \rightarrow C_6A\$_3H_{32} + 2AH_3 \quad (3)$$

As mentioned above, the amounts of $C_{12}A_7$, CA and C_4A_3\$ reacting were calculated on the assumption that β-C_2S percentage remained invariant. So, the ratio between crystalline phases at the same hydration time must be constant and it is mathematically expressed in (4):

$$\frac{\beta - C_2S(t_{0.6})_R}{\text{Aluminate}(t_{0.6})_R} = \frac{\beta - C_2S(t_0)_N}{\text{Aluminate}(t_0)_N - X} \quad (4)$$

where β-$C_2S(t_{0.6})_R$ and aluminates$(t_{0.6})_R$ stand for Rietveld percentages of β-C_2S, and $C_{12}A_7$, CA or C_4A_3\$ phases, respectively, at 0.6 h (Table 6). On the other hand, β-$C_2S(t_0)_N$ and aluminates$(t_0)_N$ stand for percentages of these phases at normalized t_0, and X is the amount of aluminate reacted at 0.6 h. In this example, X was 1.9 for $C_{12}A_7$, 0.1 for CA and −0.3 for C_4A_3\$. The (small) negative value for C_4A_3\$ indicates that this phase does not react during this time. Thus the total amount of water reacting, considering only Eqs. (1) and (2), was 2.4 wt.%. These first reactions assume that AH_3 is formed. However, crystalline AH_3 was not identified by XRPD. In literature this phase is often reported to be based on

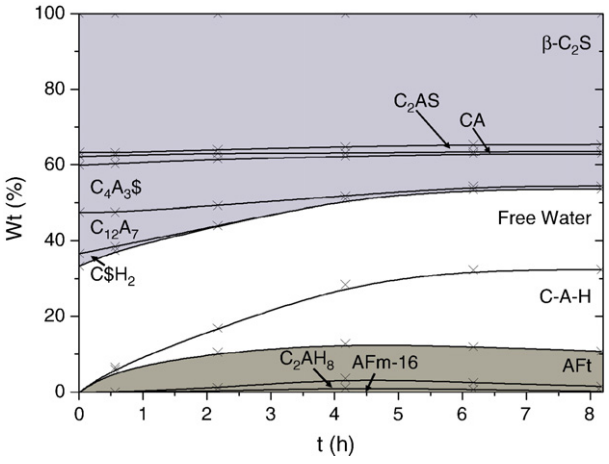

Fig. 6. Normalized quantitative phase analysis results for C5BSA_60:20 paste up to 8.2 h from LXRPD data.

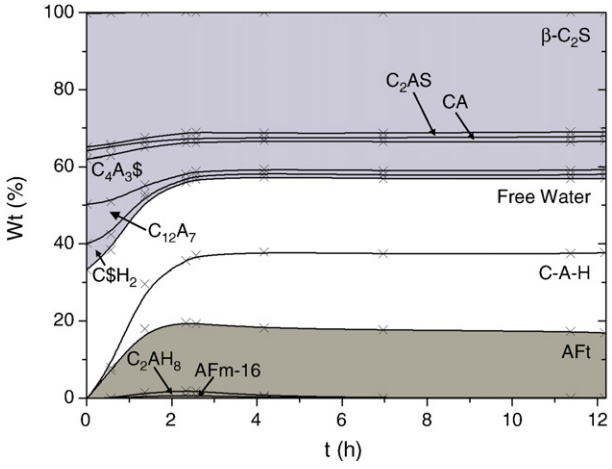

Fig. 7. Normalized quantitative phase analysis results for C10BSA_60:20 paste up to 15.2 h from LXRPD data.

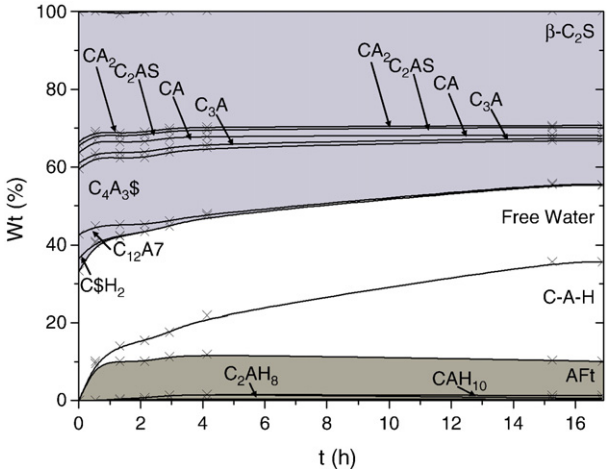

Fig. 8. Normalized quantitative phase analysis results for C5BSA_50:30 paste up to 16.9 h from LXRPD data.

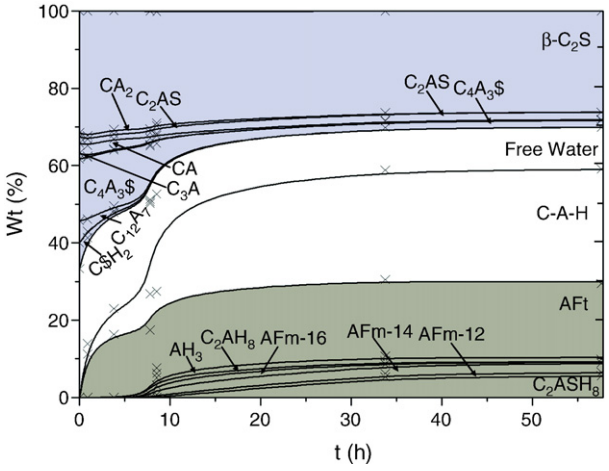

Fig. 9. Normalized quantitative phase analysis results for C10BSA_50:30 paste up to 57.6 h from SXRPD data.

hydrous alumina using the term "AH_3" [66] and it is considered as ill-crystallized or amorphous phase at early stages. Therefore, using stoichiometric constraints and the *X* value previously calculated, the total amount of amorphous AH_3 derived in this step was 0.6 wt.%. Finally, to re-normalize at $t_{0.6}$, direct Rietveld results are recalculated to include 30.9 wt.% (33.3 wt.%–2.4 wt.%) of free water and 0.6 wt.% of amorphous-AH_3. This strategy was followed to normalize each RQPA results, for C5BSA_60:20 up to $t_{8.2}$. Fig. 10 shows the Rietveld plot for C5BSA_60:20 at $t_{4.2}$, as an example of a cement paste. Main diffraction peaks of AFt, $C_4A_3\$$ and β-C_2S are labeled.

In the acceleration period, when gypsum is consumed or a passive precipitate of other phases cover the particle surfaces, the formation of ettringite is stopped and the following hydration reactions start to take place:

$$C_{12}A_7 + 51H \rightarrow 6C_2AH_8 + AH_3 \quad (5)$$

$$2CA + 11H \rightarrow C_2AH_8 + AH_3 \quad (6)$$

$$2C_3A + 27H \rightarrow C_2AH_8 + C_4AH_{19} \quad (7)$$

$$C_4A_3\$ + 18H \rightarrow C_4A\$H_{12} + 2AH_3 \quad (8)$$

$$C_4A_3\$ + 22H \rightarrow C_4A\$H_{16} + 2AH_3 \quad (9)$$

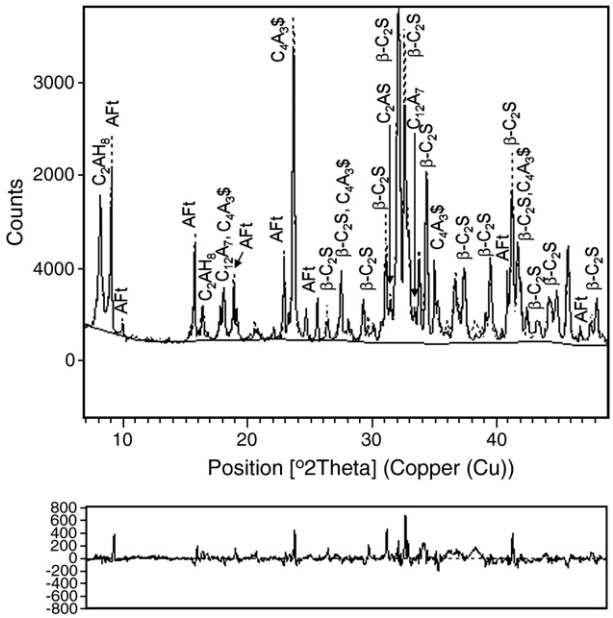

Fig. 10. Selected range of the LXRPD Rietveld plot for C5BSA_60:20 paste after 4.2 h of hydration. Dots are the experimental data, solid line is the calculated pattern and the difference curve is given at the bottom. The major peaks for each phase are labeled.

Additionally, CAH_{10} appears in the C5BSA_50:30 cement pastes at later ages, which we assume is due to the following reaction:

$$CA + 10H \rightarrow CAH_{10} \quad (10)$$

$C_4A\$H_{12}$ and $C_4A\$H_{16}$, hereafter named as AFm-12 and AFm-16, respectively, belong to an isostructural group of compounds (AFm-phases). These compounds have a layer structure with general formula $[Ca_2Al(OH)_6]X \cdot xH_2O$ where *X* denotes one formula unit of a singly charged anion (for instance OH^-) or half a formula unit of a doubly charged anion (for instance SO_4^{2-}) placed within the interlayer space jointly with water molecules. The presence of phases with different layer spacings is justified twofold: i) by the partial anion replacement OH^-/SO_4^{2-} within the AFm phases; and ii) by the progressive release of the water molecules as a consequence of the hydration of other phases. For instance, AFm-12 interlayer spacing is variable between 8.2 and 8.9 Å since it forms a solid solution where the SO_4^{2-} groups may be partly replaced by OH^- anions. After several hours of hydration, $C_4A\$H_{14}$ (AFm-14) also appears, presumably by dehydration of AFm-16, see Eq. (11). On the other hand, β-C_2S starts to react but does not simply react with water, as portlandite does not appear. Instead, it reacts with gibbsite to yield stratlingite (C_2ASH_8) according to reaction (12). It must be noted that gehlenite itself is thought not to hydrate as its direct RQPA content increases with time.

$$C_4A\$H_{16} \rightarrow C_4A\$H_{14} + 2H \quad (11)$$

$$C_2S + AH_3 + 5H \rightarrow C_2ASH_8 \quad (12)$$

The crystal structure published in [56] for AFm-12 has been used to fit and quantify AFm-14 and AFm-16 phases by adjusting their *c*-values. CAH_{10} phase has been quantified using the structural description published in [57]. Fig. 11 shows the low angle region of the SXRPD Rietveld plot for C10BSA_50:30 cement at $t_{33.8}$. Main peaks in this region have been labeled including the basal d-spacings. AFm-12, AFm-14 and AFm-16 have the interlayer d-spacings at 8.3, 9.5 and 10.3 Å, respectively [13]. It is also well known that C_2AH_8 is an AFm-type phase with an interlayer d-spacing close to 10.7 Å [70,71]. We have used

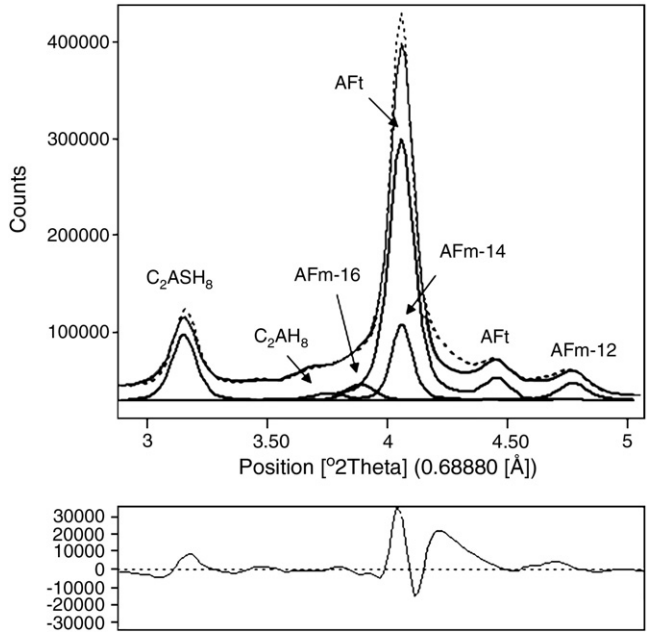

Fig. 11. Low angle detail of the SXRPD Rietveld plot for C10BSA_50:30 paste after 33.8 h of hydration. Dots are the experimental data, solid line is the calculated pattern and the difference curve is given at the bottom. Individual patterns, from each crystalline phase, have been included and labeled.

the crystalline phase ratios to elucidate the reactivity of $C_{12}A_7$, CA and C_3A to form C_2AH_8 according to Eqs. (5), (6) and (7) and $C_4A_3\$$ to form AFm-12 or AFm-16 according to (8) and (9) reactions.

C_2AH_8 is a metastable AFm-type phase and there is no full structural description available. To fit the diffraction peaks arising from this phase, we have used an average hexagonal structural description, s. g. $P6_122$, with $a = b = 5.7880$ Å and $c = 64.5018$ Å, to be reported elsewhere. This structure has been obtained by SXRPD *ab initio* structure determination from a sample with other crystalline phases. We have to highlight that two hydrate aluminates are formed in reaction (7), C_2AH_8 and C_4AH_{19}. X-ray patterns of these two phases are almost coincident, so we have quantified both as one phase, with C_2AH_8 stoichiometry. The amount of C_2AH_8 increases slightly with time, reaching a maximum for C5BSA_60:20 at $t_{3.8}$. However, higher hydration times produce a decrease of its content, disappearing completely at later ages.

To conclude the normalization, it is necessary to mention that the determined crystalline percentages of AFm-type phases by Rietveld method are smaller than those derived from the consumption of $C_{12}A_7$, CA, C_3A or $C_4A_3\$$. Therefore, amorphous calcium aluminum hydrates of unknown composition, written generically as C-A-H, have to be included from this indirect observation [72].

The formation of AFm-type phases has been also confirmed by calorimetric studies. Fig. 12 shows a selected range (0–20 h) of the heat flow (power) and overall heat evolution (enthalpy) curves for the four studied pastes. Signal for the first 45 min of hydration were not recorded due to experimental requirements for stabilization. The main acceleration period starts between 1 and 3 h after mixing. Two broad power peaks are observed for all pastes in the interval from 1 to 10 h. The first broad signal is likely associated with ettringite and C-A-H gel formation. The remaining signals (in the 5–7 h interval) are likely related to C-A-H gel and AFm-type phases formation. The overall heat evolved for C5BSA_60:20, C10BSA_60:20, C5BSA_50:30 and C10BSA_50:30 cements for 110 h were: 232, 215, 277 and 244 J/g, respectively. For any given clinker, a decrease of the total heat evolved

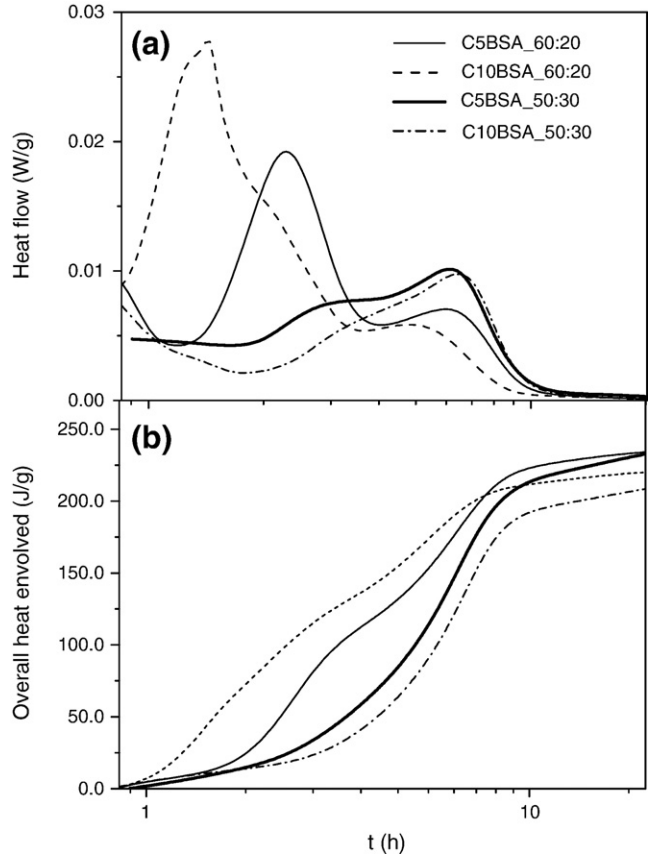

Fig. 12. Selected range of calorimetric heat flow and overall evolved heat curves for the studied pastes.

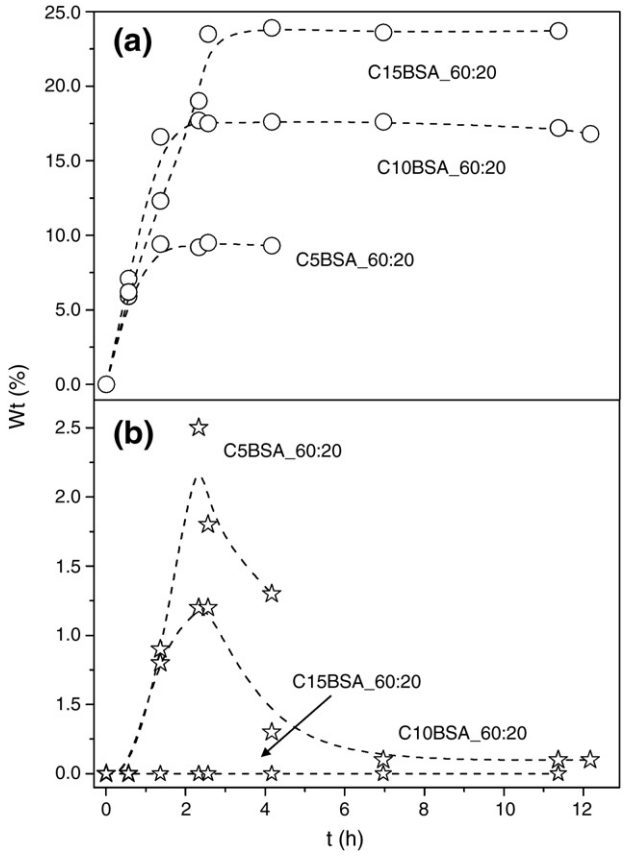

Fig. 13. Evolution of (a) ettringite and (b) C_2AH_8 in the indicated pastes.

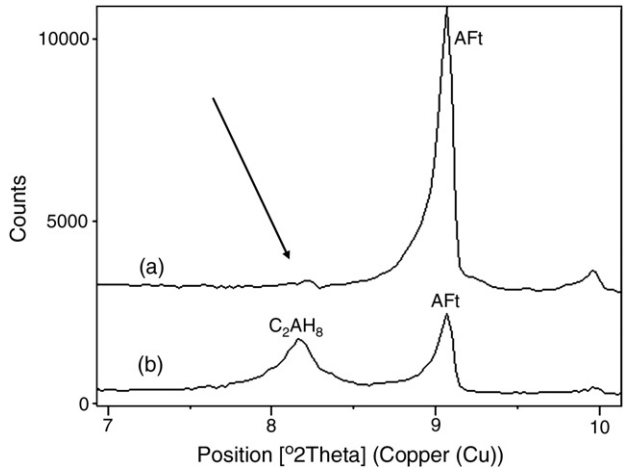

Fig. 14. Low angle detail of LXRPD patterns for (a) C10BSA_50:30 paste and (b) C5BSA_50:30 paste, at 4.2 h. Main peaks for AFt and C_2AH_8 phases have been labeled. The arrow highlights the absence of C_2AH_8 phase in (a).

at a give time is observed when the amount of added gypsum increases. This behavior is probably mainly due to the reduction in the content of anhydrous cement phases if more gypsum is added. On the other hand, all of these cements show higher hydration enthalpies than a typical belite-rich cement (with no $C_4A_3\$$ but with some C_3S) which was slightly lower than 190 J/g at 6 days (144 h) [10].

The effect of the amount of added gypsum on the hydration process was also investigated. To do so, C15BSA_60:20 paste was also prepared and studied. Fig. 13a and b shows the ettringite and C_2AH_8 phase evolutions with the time for C5BSA_60:20, C10BSA_60:20, and C15BSA_60:20 cements. Ettringite formation is favored in cement with 15 wt.% of gypsum added, according to reactions (1), (2), and (3), shown above; conversely, the amount of C_2AH_8 is higher in the cements with less gypsum. Related to this behavior, Fig. 14a and b shows the low angle region of the LXRPD patterns for C10BSA_50:30 and C5BSA_50:30 at $t_{4.2}$, respectively. Even the most intense diffraction peak of C_2AH_8 phase is barely visible in the cement with 10 wt.% gypsum.

Finally, after the quantitative phase analysis and the normalization step, the degree of reaction of selected phases can be calculated at a given time according to (13). Table 10 shows the degree of reaction for selected phases at early ages (up to ~17 h) for C5BSA_60:20, C10BSA_60:20 and C5BSA_50:30 cements and at later ages (~34 h, and ~58 h) for C10BSA_50:30.

Several conclusions can be inferred by inspecting Table 10: i) β-C_2S begins to hydrate at early ages (~34 h) compared with belite-rich cements [73], ii) $C_{12}A_7$ reacts with water faster than the other aluminates (C_3A, $C_4A_3\$$, CA and CA_2) in C5BSA_60:20, C10BSA_60:20 and C5BSA_50:30 cements and at the same rate as C_3A in C10BSA_50:30 (in this case, both phases disappear completely at 8.5 h), and finally iii) $C_4A_3\$$ hydration is strongly affected by the amount of gypsum added, as expected. This phase reacts more slowly in cements with 5 wt.% of gypsum, because almost all of the gypsum is very rapidly consumed by the hydration of $C_{12}A_7$. On the other hand, in cements with 10 wt.% of gypsum the degree of reaction is much larger during the first 2 h.

$$\text{Degree of reaction of phase}-n\ (\%) = \frac{W^{t0}_{\text{phase}-n} - W^{t}_{\text{phase}-n}}{W^{t0}_{\text{phase}-n}} \times 100 \quad (13)$$

4. Conclusions

The burnability of raw mixtures for making aluminum-rich belite sulfoaluminate clinkers has been studied by TG-DTA, HTM and X-ray powder diffraction with Rietveld quantitative phase analysis. 15 min at 1350 ºC was found to be sufficient for good clinkering. Under these conditions, the amounts of $C_4A_3\$$ found in the resulting BSA clinkers were very close to the target values. Full quantitative phase analyses are reported for the three clinker compositions tested. However, more research is needed in order to understand all of the reactions taking place in the production of these clinkers. Although partial inhibition of C_2AS formation is obtained in the presence of SO_3, there were small percentages of this phase in all of the laboratory BSA clinkers made here.

Phase assemblage evolution with time during the hydration of BSA cements made from the above clinkers with added gypsum was determined by normalization of Rietveld results taking into account free water and amorphous phases that appear during hydration. QPA of synchrotron diffraction data for C10BSA_50:30 cement shows that β-C_2S reacts at early ages (33.8 h) compared to a belite-rich Portland cement (in which this phase does not react during the first three months). The early hydration of β-C_2S in these BSA cements is not the usual reaction to yield C-S-H gel and portlandite, as portlandite is not detected in the pastes. Instead, belite appears to react with amorphous AH_3 to yield stratlingite. On the other hand, the aluminate phases react faster than the Klein's salt, which hydrates at a higher pace than belite phases. The hydration mechanisms of the aluminate phases in these clinkers are shown to be strongly dependent on the initial amount of gypsum added. A methodology to simultaneously quantify several different AFm phases is also reported.

Acknowledgments

We thank Dr. A.H. De Aza (ICV-CSIC, Madrid) for his help during the high-temperature microscopy study. We also thank financial support from P06-FQM-01348 research grant (Junta de Andalucía, Spain). ESRF is thanked for the provision of X-ray synchrotron powder diffraction beam time. We also thank Dr. Marco Merlini (University of Milan) for his help during the synchrotron X-ray experiment.

References

[1] J.S. Damtoft, J. Lukasik, D. Herfort, D. Sorrentino, E.M. Gartner, Sustainable development and climate change initiatives, Cem. Concr. Res. 38 (2) (2008) 115–127.
[2] E. Gartner, Industrially interesting approaches to "low CO_2" cements, Cem. Concr. Res. 34 (9) (2004) 1489–1498.
[3] A.K. Chatterjee, High belite cements. Present status and future technological options: Part I and Part II, Cem. Concr. Res. 26 (8) (1996) 1213–1237.
[4] A.G. De la Torre, M.A.G. Aranda, A.H. De Aza, P. Pena, S. De Aza, Belite portland clinkers. Synthesis and mineralogical analysis, Bol. Soc. Esp. Ceram. Vidr. 44 (3) (2005) 185–191.

Table 10
Degree of reaction (%) for clinker phases in the pastes at selected times.

Phase	C5BSA_60:20		C10BSA_60:20			C5BSA_50:30			C10BSA_50:30			
	2 h	8 h	2 h	7 h	12 h	2 h	4 h	17 h	4 h	9 h	34 h	58 h
β-C_2S	0	0	0	0	0	0	0	0	0	0	17	17
$C_{12}A_7$	51	93	86	88	88	68	92	97	79	100	100	100
C_3A	–	–	–	–	–	0	33	60	80	100	100	100
CA	30	70	52	52	52	0	30	70	0	81	92	92
$C_4A_3\$$	2	32	32	37	38	0	0	34	9	86	89	89

[5] C.D. Popescu, M. Muntean, J.H. Sharp, Industrial trial production of low energy belite cement, Cem. Concr. Compos. 25 (7) (2003) 689–693.
[6] F.P. Glasser, L. Zhang, High-performance cement matrices based on calcium sulfoaluminate-belite compositions, Cem. Concr. Res. 31 (2001) 1881–1886.
[7] L. Zhang, M.Z. Su, Y.M. Wang, Development of the use of sulfo- and ferro-aluminate cements in China, Adv. Cem. Res 11 (1999) 15–21.
[8] J. Stark, A. Muller, R. Seydel, K. Jost, Conditions of the existence of hydraulically active belite cement, Proceedings of the 8th International Congress of Cement Chemistry, Rio de Janeiro, vol. II, 1986, pp. 306–309.
[9] A. Gies, D. Knofel, Influence of alkalies on the composition of belite-rich cement clinkers and the technological properties of the resulting cements, Cem. Concr. Res. 16 (3) (1986) 411–422.
[10] K. Morsli, A.G. de la Torre, S. Stöber, A.J.M. Cuberos, M. Zahir, M.A.G. Aranda, Quantitative phase analysis of laboratory active belite clinkers by synchrotron powder diffraction, J. Am. Ceram. Soc. 90 (10) (2007) 3205–3212.
[11] K. Morsli, A.G. de la Torre, M. Zahir, M.A.G. Aranda, Mineralogical phase analysis of alkali and sulfate bearing belite rich laboratory clinkers, Cem. Concr. Res. 37 (2007) 639–646.
[12] G.S. Li, E.M. Gartner, High-belite sulfoaluminate clinker: fabrication process and binder preparation, French patent application 04-51586 (publication 2873366), 27/01/2006.
[13] H.F.W. Taylor, Cement Chemistry, Thomas Telford, London, 1997.
[14] K. Quillin, Performance of belite-sulfoaluminate cements, Cem. Concr. Res. 31 (2001) 1341–1349.
[15] C.D. Lawrence, The production of low-energy cements, in: J. Bensted, P. Barnes (Eds.), Structures and performance of cements, Spon Spress, London, 2002.
[16] I. Janotka, U. Krajci, S.C. Mojumdar, Performance of sulphoaluminate–belite cement with high $C_4A_3$$ content, Ceram.-Silik. 51 (2007) 74–81.
[17] D. Adolfsson, N. Menad, E. Viggh, B. Bjorkman, Hydraulic properties of sulphoaluminate belite cement based on steelmaking slags, Adv. Cem. Res 19 (2007) 133–138.
[18] J. Pera, J. Ambroise, New applications of calcium sulfoaluminate cement, Cem. Concr. Res. 34 (2004) 671–676.
[19] A. Wolter, Belite cements and low energy clinker, Cem. Int. 3 (2005) 106–117.
[20] G.L. Valenti, M. Marroccoli, F. Montagnaro, M. Nobili, A. Telesca, Synthesis, hydration properties and environmental friendly features of calcium sulfoaluminate cements, Proceedings of the 12th International Congress of Cement Chemistry, Montreal, 2007, W3 11.2.
[21] Y.B. Pliego-Cuervo, F.P. Glasser, The role of sulphates in cement clinkering: subsolidus phase relations in the system $CaO–Al_2O_3–SiO_2–SO_3$, Cem. Concr. Res. 9 (1979) 51–56.
[22] P. Arjunan, M.R. Silsbee, D.M. Roy, Sulfoaluminate–belite cement from low-calcium fly ash and sulfur-rich and other industrial by-products, Cem. Concr. Res. 29 (1999) 1305–1311.
[23] H. Li, D.K. Agrawal, J. Cheng, M.R. Silsbee, Microwave sintering of sulphoaluminate cement with utility wastes, Cem. Concr. Res. 31 (2001) 1257–1261.
[24] F.P. Glasser, L. Zhang, Calculation of the chemical water demand for hydration of calcium sulfoaluminate cement, Proceedings of the 4th Beijing International Symposium on Cement and Concrete, vol. 3, International Academic Publishers, Beijing, 1998, pp. 97–108.
[25] F.P. Glasser, L. Zhang, Hydration of calcium sulfoaluminate cement at less than 24 h, Adv. Cem. Res 11 (1) (1999) 35–41.
[26] H.M. Rietveld, A profile refinement method for nuclear and magnetic structures, J. Appl. Crystallogr. 2 (2) (1969) 65–71.
[27] A.G. De la Torre, A. Cabeza, A. Calvente, S. Bruque, M.A.G. Aranda, Full phase analysis of Portland clinker by penetrating synchrotron powder diffraction, Anal. Chem. 73 (2001) 151–156.
[28] N.V.Y. Scarlett, I.C. Madsen, C. Manias, D. Retallack, On-line X-ray diffraction for quantitative phase analysis: Application in the Portland cement industry, Powder Diffr. 16 (2) (2001) 71–80.
[29] A.G. De la Torre, M.A.G. Aranda, Accuracy in Rietveld quantitative phase analysis of Portland cements, J. Appl. Crystallogr. 36 (5) (2003) 1169–1176.
[30] V.K. Peterson, A.S. Ray, B.A. Hunter, A comparative study of Rietveld phase analysis of cement clinker using neutron, laboratory X-ray, and synchrotron data, Powder Diffr. 21 (1) (2006) 12–18.
[31] L. León-Reina, A.G. De la Torre, J.M. Porras-Vázquez, M. Cruz, L.M. Ordonez, X. Alcobé, F. Gispert-Guirado, A. Larrañaga-Varga, M. Paul, T. Fuellmann, R. Schmidt, M.A.G. Aranda, Round robin on Rietveld quantitative phase analysis of Portland cements, J. Appl. Crystallogr. 42 (2009) 906–916.
[32] A.G. De la Torre, S. Bruque, M.A.G. Aranda, Rietveld quantitative amorphous content analysis, J. Appl. Crystallogr. 34 (2001) 196–202.
[33] K.L. Scrivener, T. Fullmann, E. Gallucci, G. Walenta, E. Bermejo, Quantitative study of Portland cement hydration by X-ray diffraction/Rietveld analysis and independent methods, Cem. Concr. Res. 34 (9) (2004) 1541–1547.
[34] C. Hesse, F. Goetz-Neunhoeffer, J. Neubauer, M. Braeu, P. Gaeberlein, Quantitative *in situ* X-ray diffraction analysis of early hydration of Portland cement at defined temperatures, Powder Diffr. 24 (2009) 112–115.
[35] A.C. Jupe, X. Turrillas, P. Barnes, S.L. Colston, C. Hall, D. Häusermann, M. Hanfland, Fast *in situ* X-ray diffraction studies of chemical reactions: a synchrotron view of the hydration of tricalcium aluminate, Phys. Rev., B 53 (1996) R14697–R14700.
[36] T. Matschei, B. Lothenbach, F.P. Glasser, The AFm phase in Portland cement, Cem. Concr. Res. 37 (2007) 118–130.
[37] J. Havlica, S. Sahu, Mechanism of ettringite and monosulphate formation, Cem. Concr. Res. 22 (1992) 671–677.
[38] C. Meneghini, G. Artioli, A. Balerna, A.F. Gualtieri, P. Norby, Multipurpose imaging-plate camera for in-situ powder XRD at the GILDA beamline, J. Synchrotron Radiat. 8 (2001) 1162–1166.
[39] A.P. Hammersley, S.O. Svensson, M. Hanfland, A.N. Fitch, D. Häusermann, Two-dimensional detector software: from real detector to idealised image or two-theta scan, High Press. Res. 14 (1996) 235–248.
[40] A.C. Larson, R.B. Von Dreele, General Structure Analysis System (GSAS), Los Alamos National Laboratory Report LAUR 86-748, 2000.
[41] P. Thompson, D.E. Cox, J.B. Hasting, Rietveld refinement of Debye–Scherrer synchrotron X-ray data from Al_2O_3, J. Appl. Crystallogr. 20 (2) (1987) 79–83.
[42] L.W. Finger, D.E. Cox, A.P. Jephcoat, A correction for powder diffraction peak asymmetry due to diaxial divergence, J. Appl. Crystallogr. 27 (1994) 892–900.
[43] W.G. Mumme, R.J. Hill, G. Bushnell-Wye, E.R. Segnit, Rietveld structure refinement, crystal chemistry and calculated powder diffraction data for the polymorphs of dicalcium silicate and related phases, Neues Jahrb. Mineral. Abh. 169 (1995) 35–68.
[44] S. Udagawa, K. Urabe, M. Natsume, T. Yano, Refinement of the crystal-structure of –Ca2SiO4, Cem. Concr. Res. 10 (2) (1980) 139–144.
[45] N.J. Calos, C.H.L. Kennard, A.K. Whittaker, R.L. Davis, Structure of calcium aluminate sulphate $Ca_4Al_6O_{16}S$, J. Solid State Chem. 119 (1995) 1–7.
[46] H. Saalfeld, W. Depmeier, Silicon–free compounds with sodalite structure, Krist. Tech. 7 (1972) 229–233.
[47] W. Hoerkner, H. Mueller-Buschbaum, Zur Kristallstrucktur von $CaAl_2O_4$, J. Inorg. Nucl. Chem. 38 (5) (1976) 983–984.
[48] L. Palacios, A.G. De la Torre, S. Bruque, J.L. García Muñoz, S. García-Granda, D. Sheptyakov, M.A.G. Aranda, Crystal structures and in-situ formation study of mayenita electrides, Inorg. Chem. 46 (2007) 4167–4176.
[49] V.I. Ponomarev, D.M. Kheiker, N.V. Belov, Crystal structure of calcium dialuminate, CA_2, Kristallografiya 15 (1970) 1140–1143.
[50] P. Mondal, J.W. Jeffery, The crystal structure of tricalcium aluminate, $Ca_3Al_2O_6$, Acta Crystallogr., B 31 (1975) 689–697.
[51] M. Kimata, N. Li, The structural property of synthetic gehlenite, $Ca_2Al_2SiO_7$, Neues Jahrb. Mineral. Abh. 144 (1982) 254–267.
[52] G. Natta, L. Passerini, Soluzioni solide, isomorfismo e simmorfismo tra gli ossidi dei metallic bivalenti. Sistemi: CaO–CdO, CaO–MnO, CaO–CoO, CaO–NiO, CaO–MgO, Gazz. Chim. Ital. 59 (1929) 129–154.
[53] A. Kirfel, G. Will, Charge density in anhydrite, $CaSO_4$ from X-ray and neutron diffraction, Acta Crystallogr., B 36 (1980) 2881–2890.
[54] A.G. De la Torre, M.G. López-Olmo, C. Álvarez-Rua, S. García-Granda, M.A.G. Aranda, Structure and microstructure of gypsum and its relevance to Rietveld quantitative phase analyses, Powder Diffr. 19 (2004) 240–246.
[55] F. Goetz-Neunhoeffer, J. Neubauer, Refined ettringite (Ca6Al2(SO4)3(OH)12 26H2O structure for quantitative X-ray diffraction analysis, Powder Diffr. 21 (1) (2006) 4–11.
[56] R. Allmann, Refinement of the hybrid layer structure $[Ca_2Al(OH)_6]\cdot 0.5(SO_4)\cdot 3H_2O$, Neues Jahrb. Mineral., Monatsh. (1977) 136–144.
[57] F. Guirado, S. Galí, S. Chinchón, J. Rius, Crystal structure solution of hydrated high-alumina cement from X-ray powder diffraction data, Angew. Chem. Int. Ed. Commun. (1998) 72–75.
[58] H. Saalfeld, M. Wedde, Refinement of the crystal structure of gibbsite, $Al(OH)_3$, Z. Kristallogr. 139 (1974) 129–135.
[59] R. Rinaldi, M. Sacerdoti, E. Passaglia, Straetlingite: crystal structure, chemistry, and a reexamination of its polytype vertumnite, Eur. J. Mineral. 2 (1990) 841–849.
[60] J. Sanz, A. Madani, J.M. Serratosa, J.S. Moya, S. De Aza, Aluminium-27 and silicon-29 magic-angle spining nuclear magnetic resonance study of the kaolinite–mullite transformation, J. Am. Ceram. Soc. 71 (10) (1988) C418–C421.
[61] J. Sanz, I. Sobrados, A.L. Cavalieri, P. Pena, S. De Aza, J.S. Moya, Structural changes induced on mullite precursors by thermal treatment: A ^{27}Al MAS–NMR investigation, J. Am. Ceram. Soc. 74 (10) (1991) 2398–2403.
[62] K. Fukuda, A. Takeda, H. Yoshida, Remelting reaction of $–Ca_2SiO_4$ solid solutions confirmed in $Ca_2SiO_4–Ca_{12}Al_{14}O_{33}$ pseudobinary system, J. Am. Ceram. Soc. 31 (2001) 1185–1189.
[63] I. Odler, Special Inorganic cements, Taylor and Francis Publisher, 2000, pp. 69–74, Chapter 4.
[64] C.D. Lawrence, The production of low-energy cements, Lea's chemistry of cement and concrete Chapter 9, 1998, pp. 421–470.
[65] D. Jun-An, G. Wen-Min, S. Mu-Zhen, L. Xiu-Ying, Sulfoaluminate cement series, Proceedings of the 7th International Congress of Cement Chemistry, Paris, vol. V, 1980, pp. 381–386.
[66] K.L. Scrivener, A. Capmas, Calcium Aluminate Cements, Lea's Chemistry of Cement and Concrete Chapter 13, 1998, pp. 709–771.
[67] F. Puertas, M.T.B. Varela, S.G. Molina, Kinetics of thermal decomposition of $C_4A_3$$ in air, Cem. Concr. Res. 38 (2) (1995) 572–580.
[68] I. Odler, H. Zhang, Investigations on high SO_3 Portland clinkers and cements I. Clinker synthesis and cement preparation, Cem. Concr. Res. 26 (9) (1996) 1307–1313.
[69] L. Kacimi, A. Simon-Masseron, A. Ghomari, Z. Derriche, Reduction of clinkerization temperature by using phosphogypsum, J. Hazard. Mater. B137 (2006) 129–137.
[70] E.M. Gartner, J.F. Young, D.A. Damidot, I. Jawed, Hydration of Portland cement, in: J. Bensted, P. Barnes (Eds.), Structures and performance of cements, Spon Spress, London, 2002.
[71] N. Ukrainczyk, T. Matusinovic, S. Kurajica, B. Zimmermann, J. Sipusic, Dehydration of a layered double hydroxide-C_2AH_8, Thermochim. Acta 464 (2007) 7–15.
[72] J. Bensted, Calcium aluminate cements, in: J. Bensted, P. Barnes (Eds.), Structure and Performance of Cements, Spon Spress, London, 2002.
[73] A.J.M. Cuberos, A.G. De la Torre, M.C. Martín-Sedeño, L. Moreno-Real, M. Merlini, L.M. Ordónez, M.A.G. Aranda, Phase development in conventional and active belite cement pastes by Rietveld analysis and chemicals constraints, Cem. Concr. Res. 39 (10) (2009) 833–842.